J Supercond Nov Magn
DOI 10.1007/s10948-013-2139-y

ORIGINAL PAPER

Magnetovoltage Measurements and Hysteresis Effects in Polycrystalline Superconducting $Y_1Ba_2Cu_3O_{7-x}$/Ag in Weak Magnetic Fields

A. Altinkok · K. Kiliç · M. Olutaş · A. Kiliç

Received: 30 January 2013 / Accepted: 1 March 2013

Abstract The magnetovoltage measurements (V–H curves) with different sweeping rates (dH/dt) of the external magnetic field in Ag-added polycrystalline $YBa_2Cu_3O_{7-x}$ sample (YBCO/Ag) were investigated. The measurements of V–H curves were carried out as functions of the transport current (I) and temperature (T). Upon cycling H, all V–H curves measured for different values of I exhibit a clockwise hysteresis effects in forward region. The hysteresis effects in the V–H curve were interpreted in terms of two-level magnetic system, which considers the superposition of the external magnetic field and the local magnetic fields in the intergrain boundaries induced by magnetic dipole moment of neighbor superconducting grains. The analysis of magnetovoltage data showed that the flux trapping in the junction network has a negligible effect on the evolution of the V–H curves and the irreversibilities arise mainly from the flux trapping inside the grains. It is shown that the width of V–H curves shows a universal scaling behavior with respect to the applied current below the critical temperature T_c. The comparison of V–H curves of the YBCO/Ag sample with those of YBCO shows that adding Ag to the superconducting structure weakens the pinning properties of Josephson medium and provokes the instabilities in measured dissipation. The presence of Ag in the superconducting matrix causes marked decrease in hysteresis effects and makes the V–H curves $\mathrm{d}H/\mathrm{d}t$ dependent. At high values of dH/dt, the instabilities and plateau regions in V–H curves increase significantly as compared to those of observed in YBCO. In addition, the interrelation between the evolution of V–H curves obtained for different values of I and the critical current I_c was demonstrated experimentally.

Keywords Cuprate superconductors · Flux pinning · Magnetoresistance · Time effects

1 Introduction

Systematic experimental studies have been made to understand the physical mechanisms responsible for the hysteresis effects in the magnetoresistance of superconducting materials [1–11]. The hysteretic effects in magnetoresistance measurements appear mostly in the clockwise direction as the external magnetic field is swept up and down [2–4, 7–11]. Generally, the low- and high-field strong irreversibilities observed in polycrystalline HTSCs samples are interpreted in terms of flux trapping developing in both intergranular and intragranular regions [2–4, 7–11]. Ji et al. [3] proposed an analytical model, so-called two-level critical state model, by calculating the macroscopic and local fields for ordered and disordered polycrystalline HTSC samples. In this model, it was assumed that the flux dynamics is maintained by percolative paths through the grains. The model explains the microwave losses in granular materials and also describes the magnetic hysteresis effects. Furthermore, a model for high-field magnetoresistance of granular samples was developed by Beloborodov et al. [12], which gives a reasonable agreement with the experimental results concerning the negative magnetoresistance observed in granular superconducting Al sample [13]. Recently, Palau et al. [6] showed that the irreversibility effects arise from the return field from grains into the grain boundaries. Balaev et al. [9] reported that the broadening of the resistive transition of polycrystalline composite samples of $Y_1Ba_2Cu_3O_{7-x}+CuO$ and its magnetore-

A. Altinkok · K. Kiliç · M. Olutaş · A. Kiliç (✉)
Turgut Gulez Research Laboratory, Department of Physics, Abant Izzet Baysal University, 14280 Bolu, Turkey
e-mail: kilic_a@ibu.edu.tr

Published online: 15 March 2013

sistance measured at very low magnetic fields could be explained well by the Ambegoakar–Halperin model [14]. Zuo et al. [5] considered a similar model to explain the resistive transition and magnetoresistance effect observed in an organic superconductor (κ-(BEDT-TTF)$_2$Cu[N(CN)$_2$]Br).

We note that the transport critical current density J_c of polycrystalline high T_c-superconductors has been found strongly hysteretic at low applied magnetic fields [1, 15–17]. The intragranular flux-trapping model was developed to calculate $J_c(H)$ and fit the experimental J_c–H data in both $Y_1Ba_2Cu_3O_{7-x}$ (YBCO) and (Bi–Pb)–Sr–Ca–Cu–O (BSCCO) ceramic superconductors [15–17]. However, these models have disregarded the magnetization of the intragranular medium. In those studies, it was assumed that the superconducting grains are embedded in nonsuperconducting host, without any intergranular shielding effects. Mahel and Pivarc [4] used the two-level magnetic system model [3] to explain the hysteresis effects in magneto-resistance measurements of HTSCs under low magnetic fields in transport and magnetic measurements at different temperatures. Chen and Qian reported irreversible behavior of the critical current density $J_c(H)$ and magnetovoltage $V(H)$ of $YBa_2Cu_3O_{7-x}$ at low magnetic fields ($H < 50$ mT) [1]. The hysteresis effects in those measurements were attributed to trapped flux in the loop comprised between superconducting grains and weak links. On the other hand, the peculiar high-field hysteresis effects observed in granular type-II superconductors were explained mainly in terms of flux trapping evolving inside the grains [1–11].

Silver is widely used in fabrication of HTSCs materials as a dopant or additive material [18–29]. Adding or doping of silver into YBCO ceramics improves significantly its plastic, mechanical, and electrophysical properties [21–24]. Improvement in the flexibility and chemical stability of YBCO were reported without reduction in the superconducting transition temperature T_c [18–20]. Ag can fill the intergranular spaces and improve both mechanical and electrical properties of YBCO ceramic by reducing the weak link effects. The presence of Ag between the YBCO grains can also provide a plastic flow region and relax undesirable residual stresses in the ceramic sample resulting from the grain anisotropy of superconductors [25]. In addition, it provides conductive paths between superconducting grains and can cause an enhancement in the critical current density J_c. The improvement in J_c can be attributed either to improved coupling between the superconducting grains or to stronger pinning of the intergranular vortices induced by the presence of Ag.

In this study, systematic magnetovoltage (V–H curves) measurements were performed in Ag-added polycrystalline $YBa_2Cu_3O_{7-x}$ sample (YBCO/Ag) at selected values of the magnitude of transport current (I), temperature (T), and magnetic field-sweep rate (dH/dt) to investigate flux dynamics, the intergranular region, and weak-link profile. For a better understanding of the influence of Ag on the superconducting properties, the experimental results obtained for YBCO/Ag were compared with those of YBCO sample. The clockwise (CW) hysteresis effects in the forward region of V–H curves were observed upon cycling H. Introducing Ag into the superconducting matrix causes peculiar voltage instabilities in V–H curves, and it is shown experimentally that the instabilities decrease significantly with decreasing dH/dt. The experimental V–H data of YBCO/Ag were mainly interpreted and analyzed by considering the two-level magnetic system. The general behavior of V–H curves was also examined by considering the method proposed by Balaev et al. [8, 10, 11]. By using this method, it is possible to distinguish the contribution from both intergranular region or intragranular region to the measured dissipation in V–H curves. A residual voltage V_r appeared at $H = 0$ in V–H curves for various values of applied transport current was correlated to the critical current value of the material. In addition, the interrelation between the evolution of V–H curves obtained for different values of I and the critical current I_c was demonstrated experimentally.

2 Experiment

The polycrystalline YBCO-123 samples were prepared by the conventional solid-state reaction method [7, 26, 28] using high-purity powders of Y_2O_3, $BaCO_3$, CuO, and $AgNO_3$ (Aldrich Co). All the powders are of 99.99 % purity. The amount of Ag added was equal to 3 % weight of nominal composition of Cu into YBCO-123. Energy Dispersive Spectroscopy (EDS) analysis was carried out to investigate stoichiometry and chemical composition of the Ag-added YBCO-123 sample. EDS analysis showed that amount of silver in YBCO/Ag is ∼3 wt% of Cu. Note that this value is comparable to the amount of doping of Ag in the superconducting structure.

The transport measurements were carried out using the four-point probe technique. The prepared Ag-added YBCO and YBCO polycrystalline bulk samples were cut in the shape of rectangular prism with typical dimensions of length $\ell = 4.0$ mm, width $w = 0.8$ mm, thickness $t = 0.4$ mm by using diamond saw. The contact resistance measured was of the order of 10^{-2} Ω below T_c and 10^{-1} Ω at room temperature. All measurements were carried out under PC control via an IEEE-488 interface card. A temperature stability better than 0.01 K was maintained during the measurements (OI, ITC-503 temperature controller). The temperature was measured by using a calibrated 27 Ohm-Rhodium–Iron thermocouple (OI, Calibration number 31202). In the experiments Keithley-2182A (nanovoltmeter) with a resolution of 1 nV and Keithley 6221 (current source) were used in measuring the sample voltage and applying the current,

respectively. In all measurements under external magnetic field, the magnetic field was generated by an electromagnet (OI, N100 electromagnet).

The magnetovoltage (V–H curves) measurements on the YBCO/Ag were carried out for a constant dc transport current (I) by sweeping the external magnetic field up [field increased branch (FIB) of the forward region (FR)] and down [field decreased branch (FDB) of the forward region (FR)] in the range 0–60 mT. The V–H curve measurements were also made after the polarity of the magnetic field was reversed [reverse region (RR)]. In all V–H measurements, the applied magnetic field was perpendicular to the transport current ($\vec{H} \perp \vec{I}$). The V–H curves were measured at selected values of temperature, transport current, and magnetic field sweep rate (dH/dt).

3 Experimental Results

3.1 Magnetovoltage (V–H Curves) Measurements at Different Sweep Rates of the External Magnetic Field (dH/dt)

The microstructures of YBCO and Ag-added YBCO samples were investigated by Scanning Electron Microscopy (SEM) (JEOL 6390–LV). Figures 1(a) and 1(b) show SEM images of YBCO and Ag-added YBCO samples, respectively. It is observed that Ag particles could be preferentially distributed along intergranular region of superconducting structure forming amorphous metallic regions between grains.

Figure 2(a) shows the hysteretic V–H curves measured at $T = 88$ K for selected values of the dc transport current $I = 10$, 15, 20, 30, and 40 mA with a fixed magnetic field sweep rate $dH/dt = 0.50$ mT/s. The measurements were carried out in five stages for each value of I. The corresponding stages are observed better in the replotted of V–H curve taken for $I = 20$ mA in Fig. 2(b). The external magnetic field is cycled up (FIB) and down (FDB) in the FR, and then the external magnetic field is cycled up and down in the RR. In the final stage, the magnetic field was increased from 0 to 60 mT (FIB in the FR), and the measurement was finished at $H_{\max} = 60$ mT. In the FR, at the beginning of the measurements for FIB, the V–H curve starts from zero for all current values and reaches a nearly steady state as the magnetic field is increased toward 60 mT. As the magnetic field is decreased from $H_{\max} = 60$ mT to 0, for the FDB in the FR, a clockwise (cw) hysteresis effect appears over the whole magnetic field range considered and the sample stays in a resistive state down to $H = 0$. We note that, for $H > 30$ mT, the V–H curves are nearly reversible.

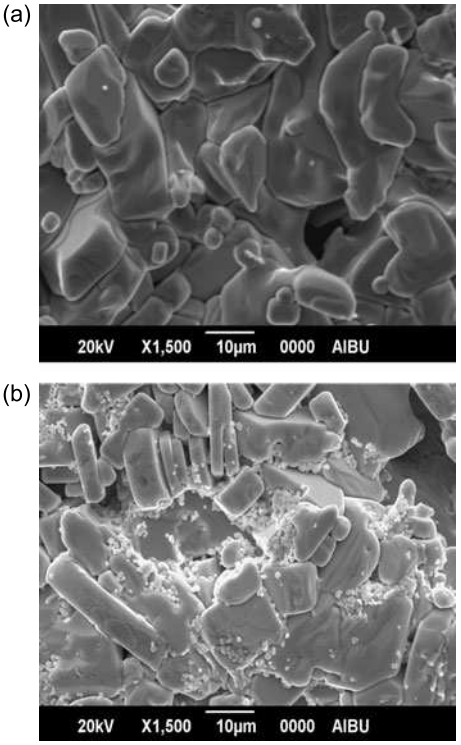

Fig. 1 SEM photomicrographs of (**a**) polycrystalline YBCO bulk sample and (**b**) Ag-added polycrystalline YBCO bulk sample. *White shiny regions* observed in SEM are the images of Ag. The magnification of SEM images is 1500

A similar case is observed in the reverse region (RR), where the polarity of magnetic field is reversed. In the third stage of V–H curves, a nonlinear increase in the measured voltage dissipation is observed, and voltage dissipation becomes approximately constant as in the FR. In the fourth stage of V–H loops, the measured dissipation decreases with decreasing the magnitude of $\vec{H}$ in the counterclockwise (ccw) direction and passes through a minimum before $\vec{H}$ becomes zero. After the minimum value, although $|\vec{H}|$ is decreased, the sample voltage increases nonlinearly and reaches a maximum value at $H = 0$. In the fifth stage of the evolution of hysteresis loops where the magnetic field is again reversed (FR), the sample voltage increases nonlinearly with increasing H and collapses on the FIB of the first stage. After the fifth stage, the plot of hysteresis loop is completed (see Fig. 2(b)). Note that the voltage drops and jumps evolve at low magnetic field values.

In order to assess the effect of dH/dt on the V–H curves, $\mathrm{d}H/\mathrm{d}t$ was increased, and the measurements described in Fig. 2 were repeated. The V–H curves measured at $T = 88$ K for $I = 15$, 20, 30, and 40 mA with $dH/dt = 1.30$ and 2.60 mT/s are presented in Figs. 3 and 4, respectively. The V–H curves in Fig. 3 exhibit a similar behavior to those in Fig. 2(a). In other words, increasing dH/dt from 0.50 mT/s to 1.30 mT/s does not cause any pronounced change in the line-shape of the V–H curves.

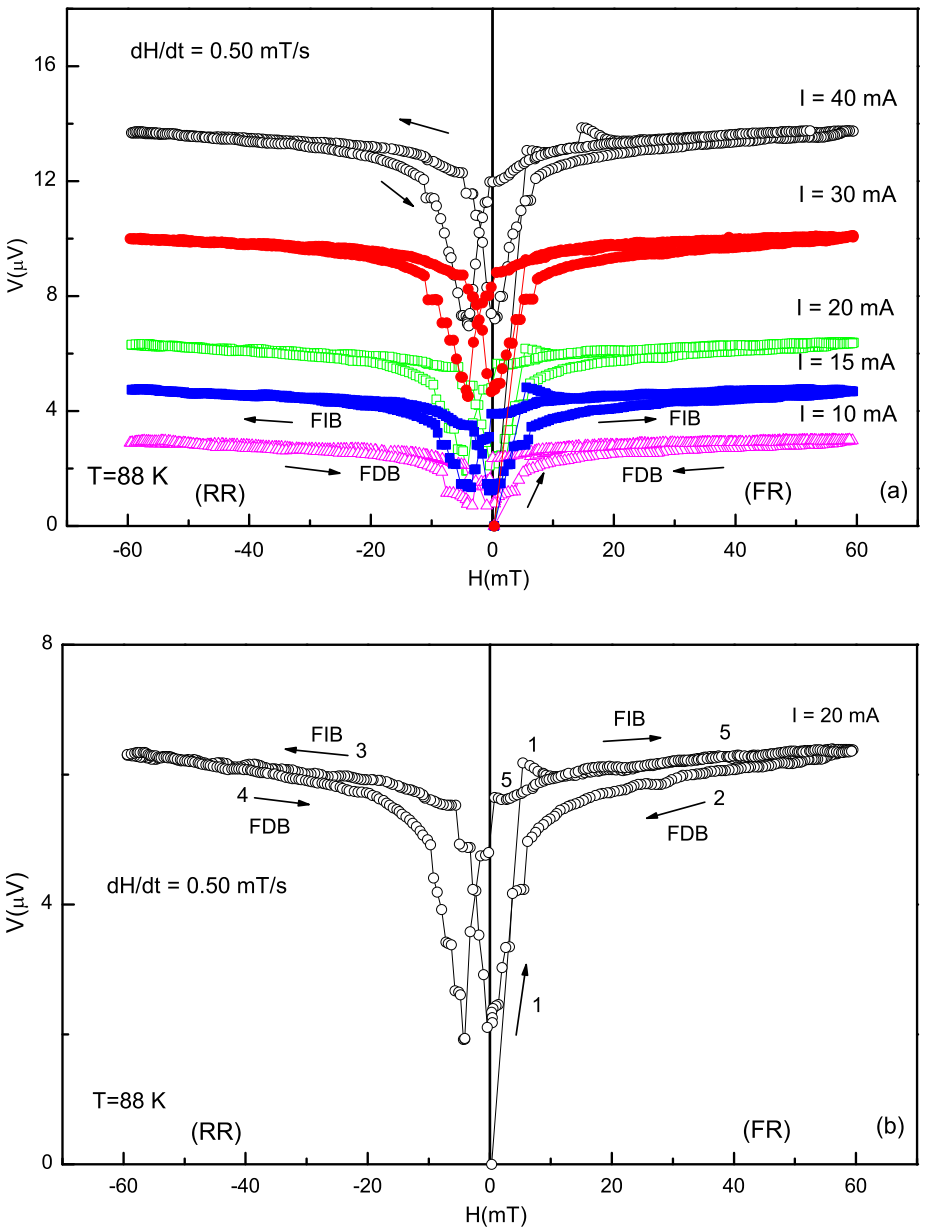

Fig. 2 (**a**) Magnetovoltage (V–H) curves of the YBCO/Ag sample measured at $T = 88$ K for selected values of the transport current, $I = 10$, 15, 20, 30, and 40 mA, with a fixed magnetic field sweep rate, $dH/dt = 0.50$ mT/s. (**b**) Replotted magnetovoltage (V–H) curve given in (**a**) for better observation of the stages of hysteresis cycle. The current is taken as $I = 20$ mA. The *arrows* show the direction of sweeping the external magnetic field

However, we note that an increase in dH/dt results in an increase in the number of the instabilities in the V–H curves. It is seen from the V–H curves given in Fig. 4 that the voltage drops and jumps and also the plateau regions are quite prominent. In addition, a comparison of V–H curves in Figs. 2–4 with each other reveals that the voltage dissipations measured at given values of I and H are practically independent of dH/dt in the range 0.50–2.60 mT/s.

In order to observe the effect of temperature on the V–H curves, the temperature was decreased from 88 to 82 K. Figures 5–7 show the V–H curves measured at 82 K and $I = 20$, 30, 40, 50, and 60 mA for $dH/dt = 0.50$, 1.30, and 2.60 mT/s, respectively. The V–H curves exhibit several different features as functions of dH/dt and transport current. For the V–H curves measured with $dH/dt = 0.50$ mT/s and $I = 20$ and 30 mA (see Fig. 5), the variation of measured dissipation with H is smooth with a few voltage drops and jumps just below 60 mT. The number of the voltage drops in the FDBs in the forward region (FR) and reverse region (RR) tends to increase with increasing the transport current (see, for instance, the FDB of V–H curve for $I = 60$ mA). In addition, as the magnetic field is decreased, the voltage measured for the FDB in FR becomes zero at $H \sim 8$ mT and 3 mT for $I = 20$ mA and $I = 30$ mA, respectively, so that below these H values the superconducting state is maintained. The V–H curves measured with $dH/dt = 1.30$ mT/s show that the voltage drops

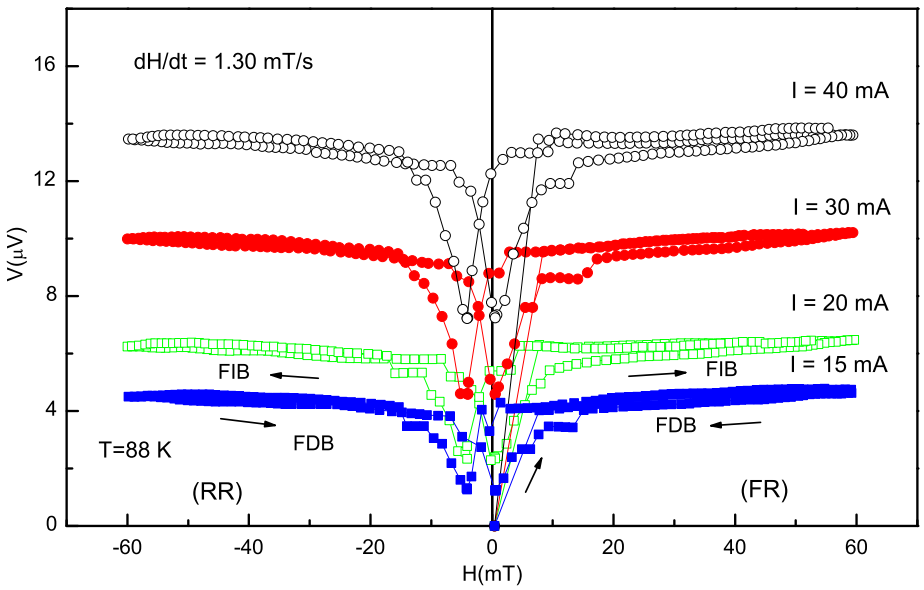

Fig. 3 Magnetovoltage (V–H) curves of the YBCO/Ag sample measured at $T = 88$ K for selected values of the transport current, $I = 15$, 20, 30, and 40 mA, with a fixed magnetic field sweep rate $dH/dt = 1.30$ mT/s. The *arrows* show the direction of sweeping the external magnetic field

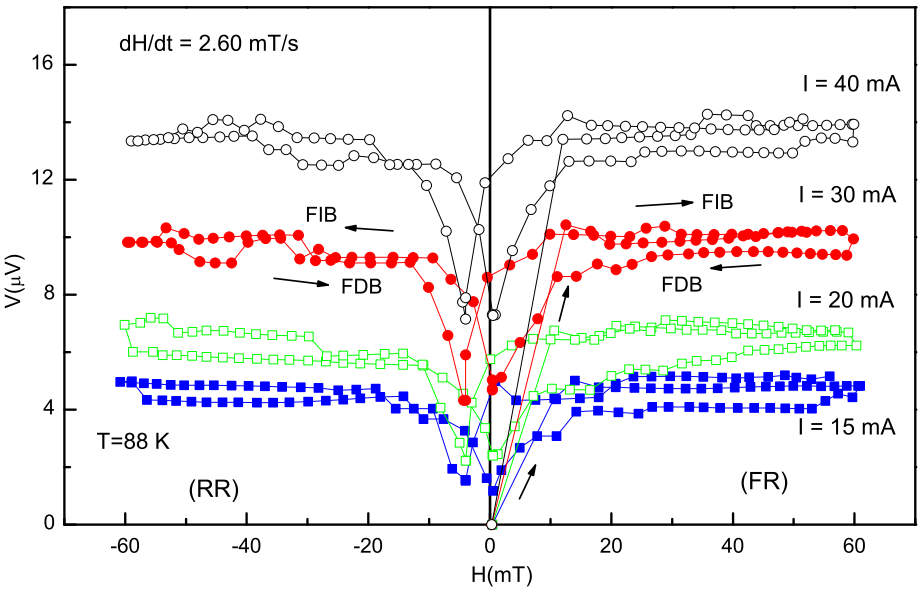

Fig. 4 Magnetovoltage (V–H) curves of the YBCO/Ag sample measured at $T = 88$ K for selected values of the transport current, $I = 15$, 20, 30, and 40 mA, with a fixed magnetic field sweep rate $dH/dt = 2.60$ mT/s. The *arrows* show the direction of sweeping the external magnetic field

and plateau regions in the FDBs of the FR and RR develop for all current values considered (Fig. 6). A further increase in dH/dt (i.e., 2.60 mT/s) results in significant instabilities as in Fig. 7. Furthermore, the symmetry in the curves obtained for the FR and RR is destroyed. However, there is no considerable change in the dissipation measured for all current values when dH/dt is increased from 0.50 to 2.60 mT/s.

Figure 8 shows a set of V–H curves of YBCO sample measured at $T = 82$ and with $I = 30$, 40, 50, and 60 mA for $dH/dt = 1.30$ mT/s. The curves exhibit several different features as a function of the transport current. One of them is the strong irreversibilities appearing upon cycling the external magnetic field. The irreversible behavior of the V–H curves for the YBCO sample is more pronounced when compared to those observed in the Ag-added YBCO sample. In the case of increasing the magnetic field for both forward and reverse directions, the resistive state becomes observable after a certain critical value of the external magnetic field, H_c^{up}, and the dissipation sharply increases and tends to saturate; whereas, in the case of decreasing the magnetic field in both forward and reverse directions, the sample becomes less resistive, and it recovers the zero resistance state at another critical value of the external magnetic field (H_c^{down}), which is much greater than H_c^{up}.

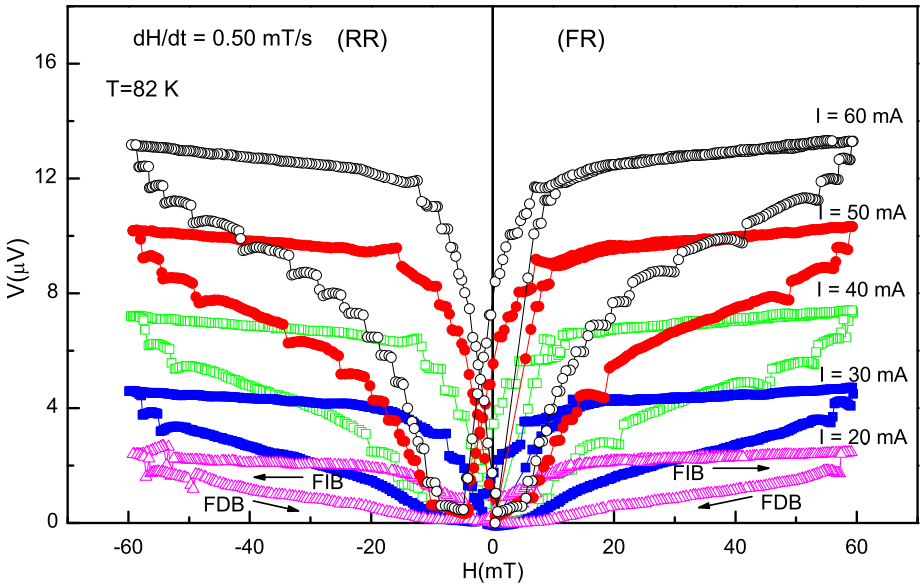

Fig. 5 Magnetovoltage (V–H) curves of the YBCO/Ag sample measured at $T = 82$ K for $I = 20$, 30, 40, 50, and 60 mA and $dH/dt = 0.50$ mT/s. The *arrows* show the direction of sweeping the external magnetic field

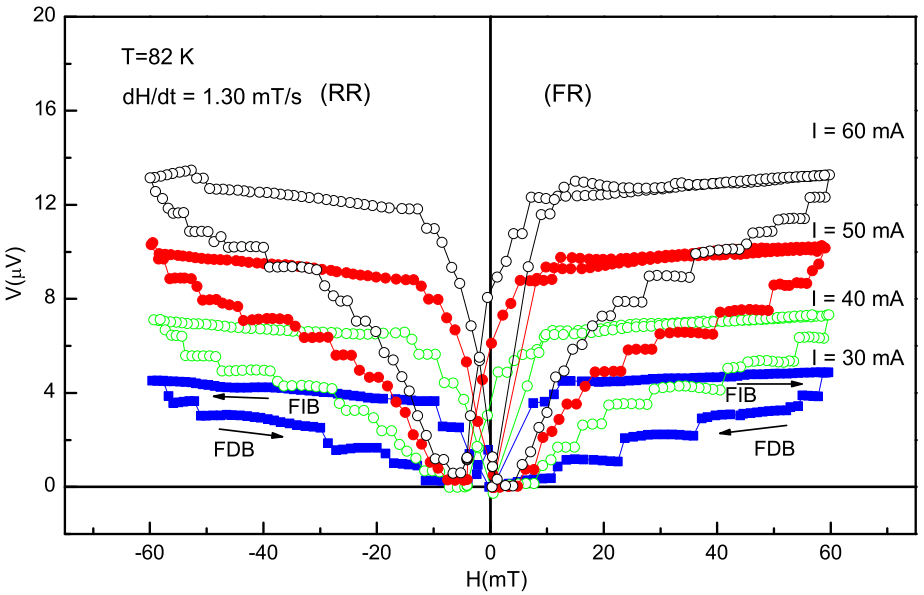

Fig. 6 Magnetovoltage (V–H) curves of the YBCO/Ag sample measured at $T = 82$ K for $I = 30$, 40, 50, and 60 mA and $dH/dt = 1.30$ mT/s. The *arrows* show the direction of sweeping the external magnetic field

4 Discussion

4.1 Microstructural Analysis

The grain size of YBCO and Ag-added YBCO samples was estimated by using SEM photomicrographs. We found that the grain size of the YBCO sample varies between 3.75–33.75 μm, whereas, for the Ag-added YBCO sample, it varies between 2.5–25 μm. The grain size of YBCO sample is generally greater than the Ag-added YBCO sample. The grain size depends mainly on annealing temperature of superconducting sample and the amount of Ag dopant [30]. It can be maximized at the temperatures just above the peritectic melting temperature of YBCO and YBCO/Ag samples. The experimental studies reveal that the peritectic temperature decreases with increasing quantity of Ag into the superconducting YBCO matrix [30]. At higher Ag content, an increase in the grain size of the superconducting phase can be observed. Ag interacts directly with YBCO during the annealing process and reduces the peritectic decomposition temperature of YBCO which is determined by the temperature at which Ag dissolves Ba and Cu from YBCO [30]. The existence of a Ba/Cu/Ag liquid solution at temperatures above the peritectic melting temperature of YBCO/Ag is assumed to play a major role in the modification of the resultant microstructure. The Ag dopant can act as a flux; on one hand, this can lead to some degree of texture of the superconducting YBCO matrix, and, on the other hand, depending on the Ag content, the increase in melt viscosity

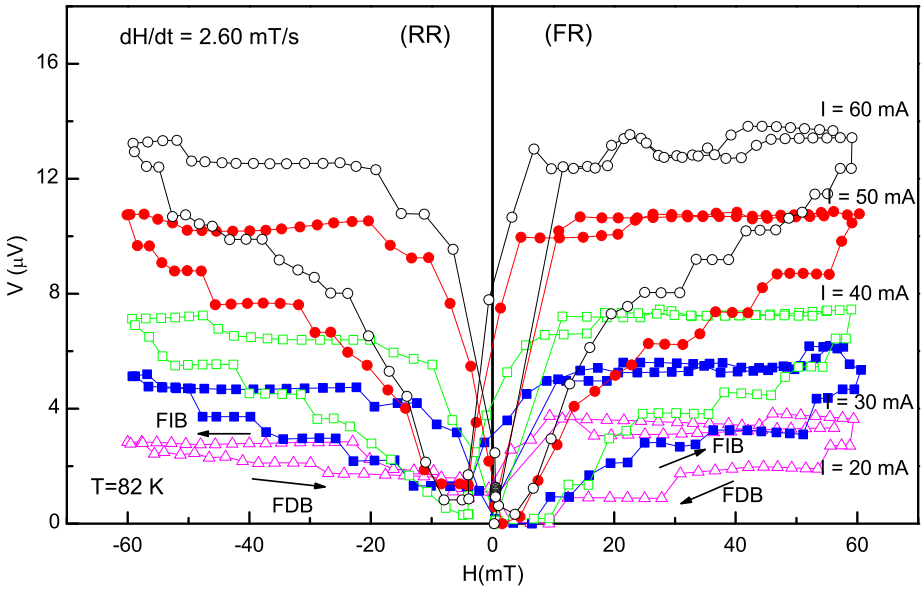

Fig. 7 Magnetovoltage (V–H) curves of the YBCO/Ag sample measured at $T = 82$ K for $I = 20$, 30, 40, 50, and 60 mA and $dH/dt = 2.60$ mT/s. The *arrows* show the direction of sweeping the external magnetic field

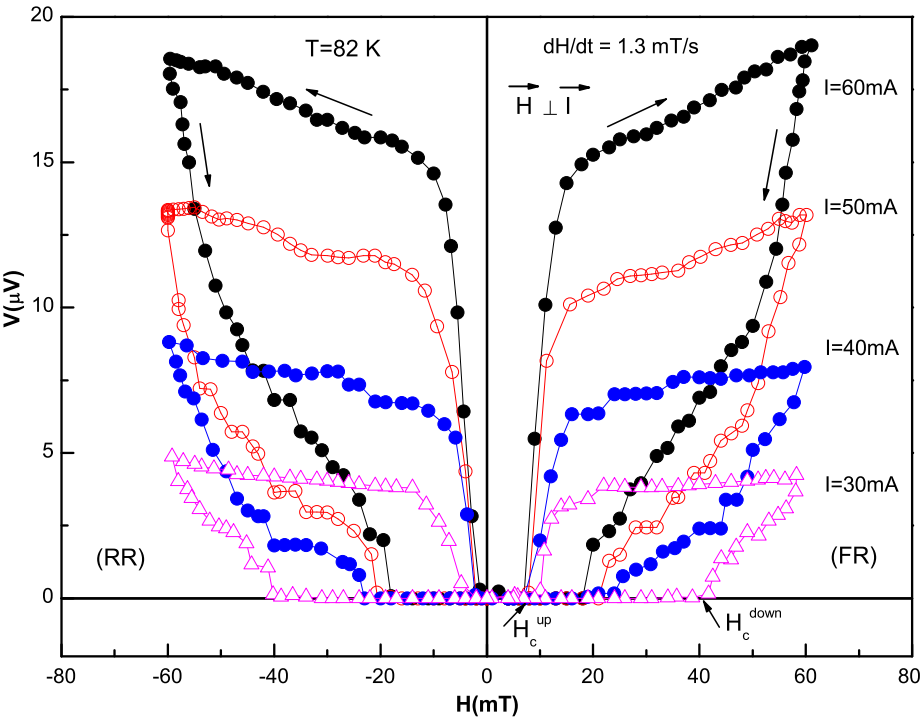

Fig. 8 Magnetovoltage (V–H) curves of the YBCO sample measured at $T = 82$ K for $I = 30$, 40, 50, and 60 mA and $dH/dt = 1.30$ mT/s. The *arrows* show the direction of sweeping the external magnetic field

can cause the formation of smaller grain size as compared to that of YBCO [30].

4.2 Hysteresis Effects in V–H Curves and Inter- and Intragranular Flux Trapping

In our measurements, the V–H curves demonstrate two distinct regimes for the field increase branch (FIB) in forward region: first, rapid increase in the measured voltage at low magnetic fields; second, at moderate field values, a saturation in the measured voltage (see Figs. 2–7). Upon cycling the external magnetic field, all V–H curves exhibit clockwise hysteresis effects that can be correlated to the two-level magnetic system.

To a first approximation, the initial rapid increase in V–H curves corresponds to the destruction of the highly ramified weak-link structure between the superconducting grains. The external magnetic field with the critical fields of weak-link structure controls predominantly the coupling states between the grains [1–4, 7, 8, 10, 11]. It should be noted that irreversibilities are related to the flux trapping in the junction network. It is well known that polycrystalline bulk

HTSC samples show typical weak-link behavior, which can be easily destroyed even at small external magnetic fields. In addition, a weak-link structure is generally assumed to behave like a type-II superconductor with its own penetration depth, H_{c1}^{W}, H_{c2}^{W}, and edge (surface like) screening current flowing along the edge of the junction, where H_{c1}^{w} and H_{c2}^{w} are the first and second critical fields of the junction network, respectively [2]. For $H > H_{c2}^{W}$, the weak link structure is completely destroyed by the external magnetic field. As H is increased above H_{c2}^{W}, the flux lines would penetrate the superconducting grains. For $0 < H \leq H_{c2}^{W}$, it is quite normal to expect that the flux lines evolve in the form of Josephson type, whereas, for $H > H_{c2}^{W}$, the flux lines penetrated into the grains will evolve gradually from Josephson to Abrikosov type with a reduced size [7, 8].

In the V–H curves, the expected resistive response of a granular sample depends on the magnitude of transport current and on the external magnetic field. At low enough applied currents less than the critical current I_c, zero resistance state is satisfied along the sample if $H < H_{c1}^{W}$, and no dissipation is observed in the V–H curves. In this case, it can be assumed that the sample behaves like a quasi-single superconducting slab and the shielding current circulates around periphery of the sample within the penetration depth λ_L. As H is increased with a certain sweep rate dH/dt, the flux lines driven by the Lorentz force associated with the transport current will penetrate the sample gradually from its surface into grain boundaries and sample pores, so that it results in an increase in the measured dissipation. At low magnetic field values, the flux motion is inhibited by the screening currents flowing between the grains surrounding by the intergranular region of the sample. When the first weak-link is broken by the flux lines in Josephson character, the critical current density increases in the neighboring area of the sample and disrupts the other weak-links as a cooperative phenomenon that we do not observe in our magnetic measurements. Thus, the density of flux lines per unit area will increase over the weak link structure, and flux motion will end in highly superconducting grains that resist strongly against the flux penetration [7]. In this process, the measured dissipation increases rapidly until the external magnetic field reaches the Josephson decoupling field, H_{c2}^{W}, of the weak-link network. If the external magnetic field is less than the first critical field of grains ($H_{c1,g}$), since $H_{c1,g} \gg H_{c2}^{W}$, further increase in the applied magnetic field up to $H_{c1,g}$ will not produce any extra dissipation because most of the grains are disconnected from each other and the intergranular region of the sample is in normal state for of $H \geq H_{c2}^{W}$. It can be assumed that, at relatively low magnetic fields, the normal state resistance of a type-II superconductor is independent of the applied magnetic field [31]. This implies that the resistance of the intergranular region will not change until the external magnetic field exceeds $H_{c1,g}$. We note that low-field M–H measurements reveal that H_{c1}^{W} and H_{c2}^{W} have values in the order of a few 0.1 mT and ∼1 mT, respectively, at liquid helium temperature [2, 7]. These junction parameters are temperature dependent and increase with decreasing temperature.

The V–H curves of YBCO (see Fig. 8) reveal that the superconducting state is not destroyed up to a critical field H_c^{up} when H is increased (for the FIB). For the FDB, the sample recovers the superconducting state at a critical magnetic field value H_c^{down} when H is decreased. The zero voltage dissipation (for the FDB branch) is a measure of reformation of the coupling between the superconducting grains. The values of H_c^{up} and H_c^{down} depend on the magnitude of transport current. For instance, for $I = 30$ mA, H_c^{down} is ∼41 mT in the V–H curve in Fig. 8 for YBCO, whereas H_c^{down} of V–H curve in Fig. 6 for the YBCO/Ag sample is ∼10 mT. This suggests that the flux pinning properties in the intergranular region of YBCO are weakened by adding Ag into the superconducting structure and enhances the formation of isolated superconducting grains in sample [18, 20, 25, 26]. This point is explained in more detail as follows: as mentioned above, the effect of addition Ag to YBCO material has been investigated extensively by several groups. Generally, a significant improvement in superconducting properties of YBCO could be obtained depending upon the content and nature of the Ag addition. In addition, the experimental studies reveal that the effective role of Ag in YBCO material depends on the processing conditions. It is well known that the field dependence of intergranular critical current density, the effective grain size, anisotropic effects associated with the misoriented grains, the compositional changes at and near grain boundaries, the distribution of pinning centers can strongly influence the low-field transport data. Further, the pinning of the vortices in a junction network depends on the amount of the disorder in the coupling strength between the grains. The addition of Ag can change structural and pinning properties of intergranular region of YBCO. First, the magnitude of the superconducting order parameter at the nonsuperconducting regions where Ag atoms exist can be suppressed locally, and such a physical case can provoke the measured dissipation. Second, the presence of randomly distributed Ag atoms cannot permit the formation of large shielding currents around the sample but can reduce them to much smaller sizes. Thus, it can make the flux motion easier from the sample surface to the interior of the sample. It can be expected that the presence of metallic regions (or paths) formed by Ag atoms along grain boundaries acts as easy motion channels for flux lines. Thus, the flux lines can move easily in those regions without encountering any obstruction until they meet highly superconducting grains, provided that the applied field is less than the first critical field of the grains (i.e., $H_{c1,g}$). This is the reason why it is observed that there is a significant difference between the H_c^{down} (and also H_c^{up}) values of Ag-added YBCO

and YBCO samples (see Fig. 6 and Fig. 8). Furthermore, addition of Ag improves the grain coupling by replacing the Josephson tunnel junctions [superconductor–insulator–superconductor (SIS)] with a large number of normal-metal proximity junctions [superconductor–normal-metal–superconductor (SNS)]. Tinkham and Lobb [32] showed analytically that the coupling energy E_J and hence intergranular critical current I_c could be less for (SNS)-type junctions than SIS tunnel junctions. It can be suggested that Ag added to YBCO reduces the intergrain coupling energy and vortex core energies leading to a pinning energy smaller than that in pure YBCO. Therefore, it can be concluded that adding Ag to YBCO can reduce the flux pinning properties of the intergranular region.

It is seen from the comparison of the V–H curves for YBCO/Ag (Fig. 6) and YBCO (Fig. 8) that the presence of Ag in the superconducting structure causes a marked decrease in hysteresis effects. In addition, the instabilities in the V–H curves of YBCO are quite small; however, the voltage drops and plateau regions in both of decreasing branches in FR and RR become more significant for the YBCO/Ag sample. The long-lived plateau regions in the decreasing branches of the V–H curves of YBCO/Ag imply that the number of flux lines joining the motion does not change and the dynamic process locks to a state for a long time, although the Lorentz forces increases. However, the opposite case observed in the V–H curves of YBCO sample means that number of the pinning centers in the junction network of YBCO is greater than that of YBCO/Ag. That is, in the case of YBCO sample, the flux lines do not lock to a state for a long time and move locally from one pinning regime to another. Thus, the dynamic process associated with the motion of flux lines in YBCO is forced to change its state gradually within a short time.

4.3 Voltage Instabilities and Field Sweep Rate (dH/dt) Dependence of V–H Curves

The number of the flux lines is controlled by the sweep rate of external magnetic field, dH/dt, which is an important parameter for the evolution of V–H curves [7]. The lowest dH/dt value used in our measurements is 0.50 mT/s, and the range of external magnetic field is between 0–60 mT. Therefore, the penetration rate of flux lines from the sample surface to its interior will be extremely large, and the weak-link network will be destroyed within a very short time, i.e., $t < 2$ s. If the grains become decoupled, a measurable voltage dissipation is observed.

As the magnetic field is decreased down to zero (FDB in the FR), it is seen from the V–H curves given in Figs. 2–4 that the measured sample voltage dissipation does not become zero. A residual voltage (V_r) at $H = 0$ that depends on I appears upon cycling H. Figure 9 shows the current

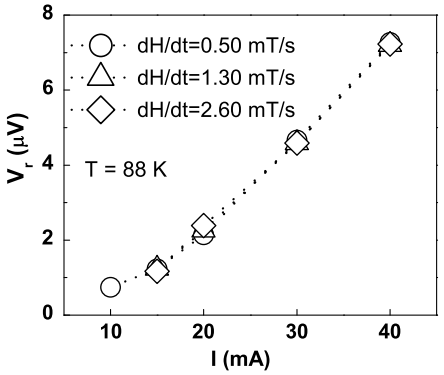

Fig. 9 Current dependence, V_r versus transport current I for YBCO/Ag at $T = 88$ K

dependence of V_r extracted from the V–H curves given in Figs. 2–4. It is seen from Fig. 9 that V_r tends to increase with I. By inspection of V_r–I curves, we suggest that the current carrying capacity of the sample (i.e., critical current I_c) can be approximately estimated. At least, the current dependence of V_r can give an idea whether the applied current I is greater than I_c or not. Further, the analysis of V–H curves measured at $T = 82$ K shows that V_r is nearly equal to zero, which implies that the applied current range of 10–40 mA is still less than I_c. It is seen from Fig. 9 that V_r becomes independent of dH/dt for $T = 88$ K. This physical case can be correlated to nearly absence of time effects at $T = 88$ K. At high temperatures, $T \sim T_c$ (i.e., $T = 88$ K), it is well known that the effective pinning forces and associated pinning potential are vanishingly small, which leads to the formation of very weak pinning disorder. For a specific value of I, it seems that the effective interaction between the flux lines and pinning centers is nearly equal each other at $T = 88$ K as dH/dt is varied from 0.50 to 2.60 mT/s. In this case, the flux lines could find enough time to move through the medium for all dH/dt values considered in these experiments. Thus, dH/dt dependence of V_r can disappear due to the less relaxation of flux lines.

It is seen from the V–H curves that the long-lived plateau regions in the decreasing branches of YBCO/Ag become more significant as dH/dt is increased from 0.50 to 2.60 mT/s. This implies that the number of the mobile flux lines does not change for a while and a constant flow rate of flux lines evolves, although the external magnetic field is continuously varied. In this process, the drop in the sample voltage is a measure of the drop in the number of flux lines and also of flux pinning. We suggest that high dH/dt values make locally the correlated flux motion unstable. However, at low values of dH/dt, the flux lines find enough time to change their states gradually, and, therefore, sharp drops or jumps are not observed in the V–H curves.

At this point, we note that the voltage drops and jumps in V–H curves do not originate from the heating effects at

current contacts that can be important in transport measurements. In order to give a measure of heating effects, it is necessary to calculate the power dissipated at the current leads. By taking the contact resistance $\sim 10^{-2}$ Ω below the critical temperature T_c and $I_{\max} = 40$ mA (see Fig. 2), we find the power dissipation at contacts as about 1.6×10^{-6} W. This would cause no marked effect on the line-shape of the V–H curves and would not be a source of instability seen in the V–H curves.

We now focus on hysteresis effects in V–H curves. The strong irreversibilities observed in low-field magnetization measurements can be taken as an indication of flux trapping in the junction network. In granular samples of HTSCs, it is generally argued that the superposition of external magnetic field and local magnetic fields (induced by magnetic dipole moment of neighbor superconducting grains in the intergrain boundaries) determines the specific character of magnetovoltage measurements [2–4, 7, 10, 11]. For the FIB in the forward region (FR), when the external magnetic field is increased with a given dH/dt, the superconducting grains will show a negative diamagnetic response to the variation of H. Within the description of the two-level magnetic system, the effective field $\vec{B}_i$ averaged over the local fields in the intergranular region will be greater than the value H [2–4, 10, 11]. On the other hand, for the FDB, when H is decreased, the diamagnetic response of superconducting grains will be positive, and the effective field B_i will be less than the value H. Therefore, the dissipation measured for the FIB and FDB at the same magnetic field value will give the result of $V(H^+) > V(H^-)$, which is the origin of the hysteresis effects observed in V–H curves (see Fig. 10) [4–6, 20, 21]. Thus, we can correlate nearly absence of irreversible behavior in the V–H curves at relatively high fields (see Figs. 2–4) to the equality of effective fields (B_{eff}) evolving in the intergranular region for the FIB and FDB. At this point, we note that the same discussion on the irreversible behavior of V–H curves is essentially valid for when the polarity of external magnetic field is reversed.

4.4 The Two-Level Magnetic System in Granular Superconductors

In the two-level magnetic system, it is assumed that the granular sample is composed of superconducting grains and weak-link junction network [2–4, 10, 11, 15, 31]. It is based on the fact of two distinct critical current densities: The larger one is locally evolving inside the grains (i.e., intragrain current density), and the other one, which is relatively lower than that in the grains, is the macroscopic intergranular current density. Since the gradient of flux density inside the grains is larger than that in the intergranular region, the analytical solution of the usual critical state model is manipulated on the basis of magnetic states associated with both intragrain and intergranular regions of the sample. The two-level magnetic system was originally proposed by Ji et al. [3] and later was extended by Mahel and Pivarc [4] to explain the hysteresis effects in HTSC cuprates. This model considers the superposition of the external magnetic field and the local magnetic fields in the intergrain boundaries induced by magnetic dipole moment of neighbor superconducting grains.

In the following, we introduce the two-level magnetic system that has been modified and adopted to HTSC cuprates by Balaev et al. [8, 10, 11]. In this model, it is assumed that the pinning in Josephson barriers (i.e., intergranular boundaries) is weak and the magnetic flux is trapped mainly in the superconducting grains. It is also assumed that the contribution of grain boundaries to the diamagnetic response of the sample is negligibly small. In this case, for $H > H_{c1}^w$, a local field $\vec{B}_i$ develops along the junction network, which is equal to the vector sum of the applied magnetic field $\vec{H}$ and the field $\vec{B}_g$ induced by the magnetization of the grains, $\vec{B}_i = \mu_0(\vec{H} + \vec{B}_g)$ or $\vec{B}_i = \mu_0(\vec{H} + G\vec{M}_g)$ since $\vec{B}_g = G\vec{M}_g$. Here G is a coefficient depending on the location and shape of the superconducting grains, and $\vec{M}_g$ is the magnetization of HTSC grains [4, 8, 10, 11, 15]. The effective field $\vec{B}_{\text{eff}}$ in the intergranular region can be found as an average of the distribution of local field $\vec{B}_i$ over all grain boundaries:

$$B_{\text{eff}} = \langle |\vec{B}_i| \rangle = \mu_o \big[H - M_g(H) f(H) \big]. \tag{1}$$

Here $f(H)$ is the average value of G over the junction network and depends on the magnitude of the external magnetic field. The magnetization $M_g(H)$ is produced by the shielding currents and the associated flux gradient evolving inside the sample.

In the case of flux trapping in junction network, the pinning of flux lines requires the magnetization of intergranular region, $\vec{M}_i$, and the local field $\vec{B}_i^w$ in the junction network that is the superposition of the external field $\vec{H}$ and the field $\vec{B}_g$ induced by the grains. In the region of grain boundaries considered, $\vec{M}_i$ makes a contribution to $\vec{B}_i^w$ opposite to that of $\vec{B}_g$. Thus, the effective field $\vec{B}_{\text{eff}}^w$ in the junction network can be found by averaging the distribution of local field $\vec{B}_i^w$ and can be written as [8]

$$B_{\text{eff}}^W = \langle |\vec{B}_i^w| \rangle = \mu_o \big(H - \big[M_g(H) f(H) - M_i(H, I) \big] \big). \tag{2}$$

At low applied magnetic field values, when the self-field induced by the transport current is comparable to the first and second critical fields H_{c1}^w and H_{c2}^w of the junction network, respectively, we note that the magnetization of intergranular region of HTSC sample (M_i) becomes current (I) dependent.

In the hysteresis loops of V–H curves, the equality of voltage values $V(H^+)$ and $V(H^-)$ corresponding to the increasing and decreasing fields H^+ and H^-, respectively,

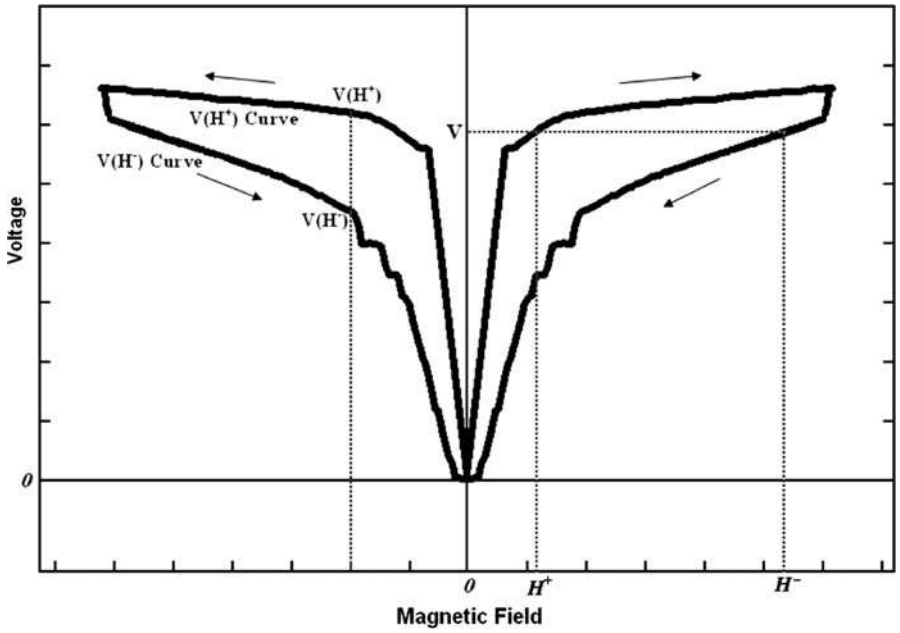

Fig. 10 Schematic plot for magnetovoltage (V–H curve). The increasing and decreasing external magnetic fields corresponding to the same sample voltage value are labeled as H^+ and H^-, respectively. ΔH is the difference between H^+ and H^- for a given value of measured sample voltage. $\Delta H = H^- - H^+$ is the width of the hysteresis loop. If $V(H^+) \neq V(H^-)$ at the same value of H, hysteresis effects appear in V–H curve

indicates the equality of effective fields, i.e., $B_{\text{eff}}(H^+) = B_{\text{eff}}(H^-)$ (see Fig. 10). When the pinning in the junction network is small, the contribution to the total magnetization from this medium will be small too, and, therefore, the equality can be written by using Eq. (1) [8]

$$H^+ - M_g\left(H^+\right) f\left(H^+\right) = H^- - M_g\left(H^-\right) f\left(H^-\right). \tag{3}$$

Thus, as is seen in Fig. 13, the width of the hysteresis loop $\Delta H = H^- - H^+$ observed in the V–H curve for a given value of measured sample voltage V can be written as

$$\Delta H = \left[M_g\left(H^-\right) f\left(H^-\right) - M_g\left(H^+\right) f\left(H^+\right)\right]. \tag{4}$$

It can be seen from Eq. (1) that the value of B_{eff} is determined only by the applied magnetic field and the magnetization of grains, and, therefore, ΔH in Eq. (4) must be independent of the transport current [8].

If the flux trapping in the intergranular medium is negligible, then it is expected that ΔH is independent of the variation in the transport current. If ΔH becomes current dependent, this may imply that there is a flux pinning in the junction network that contributes to the effective field (B^w_{eff}) in the intergranular region, and, thus, B^w_{eff} will change with the transport current. In this case, ΔH can be written as [8]

$$\begin{aligned}\Delta H = &\left[M_g\left(H^-\right) f\left(H^-\right) - M_i\left(H^-, I\right)\right] \\ &- \left[M_g\left(H^+\right) f\left(H^+\right) - M_i\left(H^+, I\right)\right].\end{aligned} \tag{5}$$

In order to observe the current dependent ΔH–H^- curves at a given temperature, the self-field induced by the transport current and the applied magnetic field must be sufficiently low and comparable to the corresponding junction parameters since $M_i \ll M_g$.

We now return to our V–H data and analyze the hysteresis effects in more detail within the method associated with the two-level magnetic system proposed by Balaev et al. [8]. Figure 11 shows the current and magnetic field sweep rate dependences of the hysteresis width (ΔH) as functions of H^-. These ΔH–H^- curves were extracted for each given current value from the V–H data in Figs. 2–4. Every extracted data point in the ΔH–H^- curves corresponds to a constant value of voltage measured in the forward region of the V–H curves (see Fig. 10). It is seen from Fig. 11(a) that all curves collapse nearly on a single curve at low field values of H^-. The departure from the single curve starts at $H^- = 6.5$, 10, and 22 mT for $dH/dt = 0.50$, 1.30, and 2.60 mT/s, respectively. We note that, for all sweep rates above these values of H^-, ΔH depends on the magnitude of transport current.

According to Eq. (5), the current dependence of ΔH can be taken as an indication of the contribution of the magnetization of intergranular region (M_i) to ΔH. On the other hand, it should be noted in Fig. 11 that the temperature ($T = 88$ K) at which the measurements were done is close to T_c. At $T \sim T_c$, the Josephson coupling energy between the grains should decrease, and, thus, the flux trapping capability of the junction network should decrease accordingly. In addition, the presence of Ag atoms in the structure causes the formation of normal regions at the grain boundaries or S–N–S junctions and can reduce enormously the Josephson coupling energy between grains. Further, as mentioned above, at a given temperature, low driving currents and low magnetic field values, which are comparable to the junction parameters, are required to observe the current dependence of ΔH.

It appears that current dependent ΔH presented in Fig. 11 is a contradiction to the intra- and intergranular flux trapping model proposed by Balaev et al. [8]. We suggest

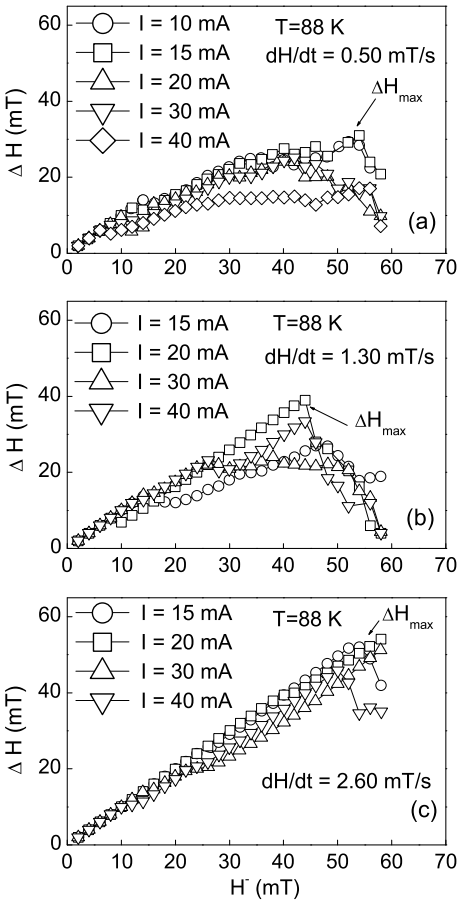

Fig. 11 ΔH–H^- curves of the YBCO/Ag sample determined at $T = 88$ K for different current values and magnetic field sweep rates: (**a**) $dH/dt = 0.50$ mT/s, (**b**) $dH/dt = 1.30$ mT/s, and (**c**) $dH/dt = 2.60$ mT/s. The data were extracted from the V–H curves in Figs. 2–4

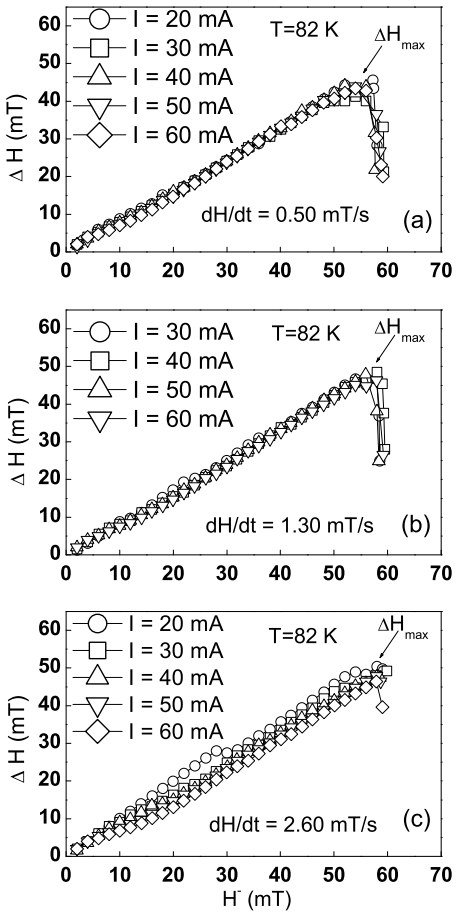

Fig. 12 ΔH–H^- curves of the YBCO/Ag sample determined at $T = 82$ K for different current values and magnetic field sweep rates: (**a**) $dH/dt = 0.50$ mT/s, (**b**) $dH/dt = 1.30$ mT/s, and (**c**) $dH/dt = 2.60$ mT/s. The data were extracted from the V–H curves in Figs. 5–7

that, at $T \sim T_c$, where the superconducting fluctuations are high, the hysteretic behavior of the V–H curves should be controlled mainly by the flux pinning in grains that are not fully superconducting regions. In this description, the percolative nature of transport current can affect weakly pinned flux lines inside the grains where the superconducting regions exist and can reinforce the depinning of the flux lines due to the Lorentz force. Therefore, a current dependence of ΔH can be expected.

Another parameter that makes ΔH current dependent is the sweep rate of external magnetic field (dH/dt). At low values of $\mathrm{d}H/\mathrm{d}t$, some of the flux lines find enough time to penetrate into the grains with the help of Lorentz force and keep their motion through the weak pinning channels by following reversible paths upon cycling the external magnetic field. However, as dH/dt is increased from 0.50 to 2.60 mT/s, the ΔH becomes approximately current independent (see Fig. 11(c)). We suggest that, at high dH/dt values, the flux penetration is prevented by the localized shielding currents circulating around the grains (negative diamagnetic response) due to the rate of variation of external magnetic field. The penetrated flux lines can be pinned by the pinning centers inside the grains and cannot find enough time to move through the grains. Thus, a relative increase in the flux pinning as compared to that observed at low values of dH/dt can evolve, which can cause relatively large irreversibility effects in the V–H curves (see Fig. 2).

Figure 12 shows that ΔH–H^- data extracted from the V–H curves given in Figs. 5–7 collapse on the same curve and are practically independent of the transport current, but depend on dH/dt. Inspection of Eq. (1) and the current independence the ΔH–H^- curves reveal that the flux trapping in grains dominates the evolution of the V–H curves. We suggest that the contribution of the pinning in junction network to the hysteresis loops at $T = 82$ K is negligible.

Figure 13 shows the variation of $\Delta H_{\max}$ with dH/dt, where $\Delta H_{\max}$ corresponds to the maximum values of the ΔH–H^- curves presented in Fig. 11 and Fig. 12. At $T = 88$ K, $\Delta H_{\max}$ increases with increasing dH/dt (Fig. 13(a)). However, this significant dependence of $\Delta H_{\max}$ on dH/dt

diminishes with decreasing the temperature from $T = 88$ to 82 K (Fig. 13(b)). This implies that the flux trapping evolving inside the grains controls the evolution of the V–H curves measured at $T = 82$ K.

Figure 14 shows the variation of ΔH with H^- determined at different transport currents for the YBCO sample. The data were extracted from the V–H curves in Fig. 8. It is seen that all data points fall on the same curve for $H^- \sim 25$ mT, except those for $I = 30$ mA. The ΔH–H^- curve determined for $I = 30$ mA follow the same curve when $H \geq 43$ mT. For $I = 30$, 40, and 50 mA, there is a current dependence of ΔH. We attribute this dependence to the flux pinning in the junction network and also to the contribution of the magnetization of intergranular region, M_i, to ΔH. Since ΔH is a measure of the difference between the forward and backward magnetizations (see Eqs. (4) and (5)), the magnetic states evolved for $I = 30$ mA should be different up to $H \sim 43$ mT as compared to those observed for other current values. In this description, the diamagnetic response of the sample reaches its highest value, and the flux penetration and motion nearly disappear for $H \sim 43$ mT.

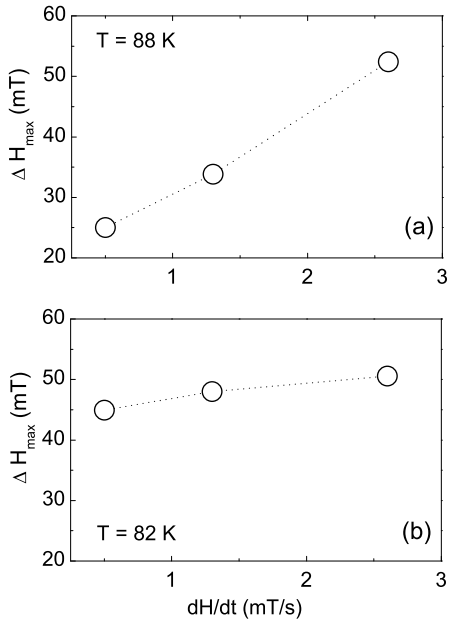

Fig. 13 The variation of $\Delta H_{\max}$ with dH/dt determined at different temperatures: (**a**) $T = 88$ K and (**b**) $T = 82$ K. $\Delta H_{\max}$ is the maximum value of the ΔH–H^- curves presented in Fig. 11 and Fig. 12

Finally, we comment on the general behavior of ΔH–H^- curves. It is seen from Fig. 12 and Fig. 14 that ΔH generally tends to increase linearly with increasing H^-. This implies that the net magnetization due to the difference between forward and backward magnetizations enhances with H^-. However a decrease in ΔH with respect to H^- can be correlated to the beginning of decrease in difference between forward and backward magnetizations. On the other hand, ΔH–H^- curves establish that the width of hysteresis loops below T_c shows a universal scaling behavior that is independent of the applied current. This means that the main mechanism controlling the hysteresis effects is the pinning of Abrikosov vortices in grains.

5 Conclusion

Systematic magnetovoltage measurements (V–H curves) were carried out in Ag-added polycrystalline $YBa_2Cu_3O_{7-x}$ (YBCO/Ag), and YBCO samples were investigated as functions of the transport current (I), sweep rate of the external magnetic field (dH/dt), and temperature (T). Upon cycling H up and down all V–H curves measured for different

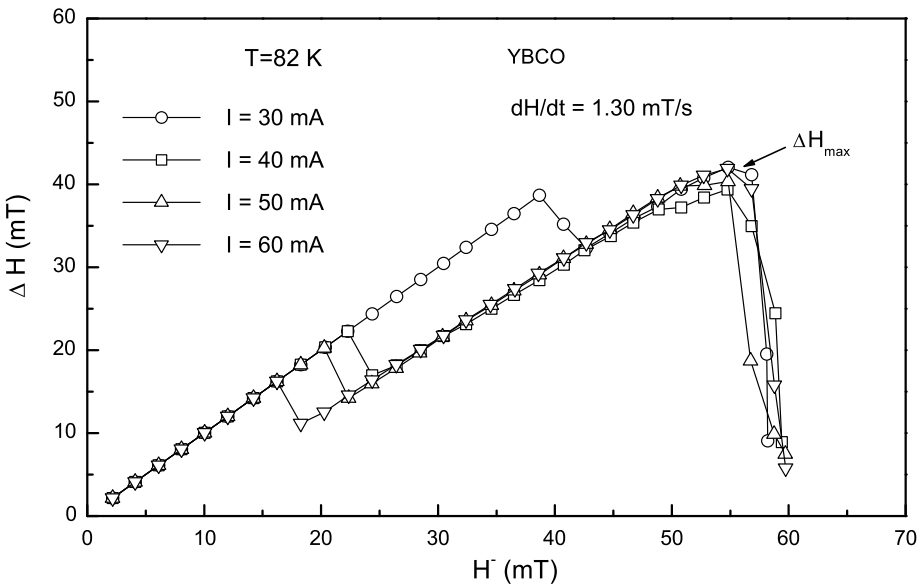

Fig. 14 ΔH–H^- curves of YBCO sample determined at $T = 82$ K for different current values and magnetic field sweep rate $dH/dt = 1.30$ mT/s. The data were extracted from the V–H curves in Fig. 8

values of I exhibit a clockwise hysteresis effects. The irreversibilities observed in the $V-H$ curves were interpreted in terms of the two-level magnetic system and were analyzed by considering a method proposed by Balaev et al. [8], which makes possible to distinguish the contribution from intergranular region or intragranular region to the measured dissipation. It is shown that the width of $V-H$ curves shows a universal scaling behavior with respect to the applied current below the critical temperature T_c. The $V-H$ curves of the YBCO/Ag sample were also compared to those of YBCO sample. Further, it was observed that introducing Ag in the superconducting structure causes to increase significantly the voltage instabilities in $V-H$ curves and makes the evolution of $V-H$ curves dH/dt dependent. At low values of $\mathrm{d}H/\mathrm{d}t$, the instabilities that reflect themselves as sharp drops or jumps are not observed in the $V-H$ curves. The analysis of the $V-H$ curves revealed that Josephson medium does not behave like a type-II superconductor due to the suppression of its pinning properties by Ag and has a negligible effect on the evolution of the $V-H$ curves. Therefore, the irreversibilities observed in $V-H$ curves arise mainly from the flux trapping inside the grains. In addition, the correlation between the evolution of $V-H$ curves obtained for different values of I and the critical current I_c was demonstrated experimentally.

References

1. Chen, K.Y., Qian, Y.J.: Physica C **159**, 131 (1989)
2. Senoussi, S.: J. Phys. III **2**, 1041 (1992)
3. Ji, L., Rzchowski, M.S., Anand, N., Tinkham, M.: Phys. Rev. B **47**, 470 (1993)
4. Mahel, M., Pivarc, J.: Physica C **308**, 147 (1998)
5. Zuo, F., Su, X., Zhang, P., Schlueter, J.A., Kelly, M.E., Williams, J.M.: Phys. Rev. B **57**, R5610 (1998)
6. Palau, A., Puig, T., Obradors, X., Pardo, E., Navau, C., Sanchez, A., Usoskin, A., Freyhardt, H.C., Fernandez, L., Holzapfel, B., Feenstra, R.: Appl. Phys. Lett. **84**, 230 (2004)
7. Kiliç, A., Kiliç, K., Yetiş, H., Çetin, O.: New J. Phys. **7**, 212 (2005)
8. Balaev, D.A., Gokhfeld, D.M., Dubrovskii, A.A., Popkov, S.I., Shaikhutdinov, K.A., Petrov, M.I.: J. Exp. Theor. Phys. **105**, 1174 (2007)
9. Balaev, D.A., Dubrovskii, A.A., Popkov, S.I., Shaikhutdinov, K.A., Petrov, M.I.: J. Supercond. Nov. Magn. **21**, 243 (2008)
10. Balaev, D.A., Gokhfeld, D.M., Dubrovskii, A.A., Popkov, S.I., Shaikhutdinov, K.A., Petrov, M.I.: J. Exp. Theor. Phys. **108**, 241 (2009)
11. Balaev, D.A., Bykov, A.A., Semenov, S.V., Popkov, S.I., Dubrovskii, A.A., Shaikhutdinov, K.A., Petrov, M.I.: Phys. Solid State **53**, 922 (2010)
12. Beloborodov, I.S., Efetov, K.B., Larkin, A.I.: Phys. Rev. B **61**, 9145 (2000)
13. Gerber, A., Milner, A., Deustscher, G., Karpovsky, M., Gladkikh, A.: Phys. Rev. Lett. **78**, 4277 (1997)
14. Ambegaokar, V., Halperin, B.I.: Phys. Rev. Lett. **22**, 1364 (1969)
15. Altshuler, E., Musa, J., Barroso, J., Papa, A.R.R., Venega, V.: Cryogenics **33**, 308 (1993)
16. Muller, K.H., Matthews, D.N.: Physica C **206**, 275 (1993)
17. Mune, P., Altshuler, E., Musa, J., Garcia, S., Riera, R.: Physica C **226**, 12 (1994)
18. Dwir, B., Affronte, M., Pavuna, D.: Appl. Phys. Lett. **55**, 399 (1989)
19. Majaros, M., Hanik, F., Polak, M., Kedrova, M.: Mod. Phys. Lett. B **3**, 981 (1989)
20. Lin, J., Chen, T.-M.: Z. Phys. B, Condens. Matter **81**, 13 (1990)
21. Lee, D.F., Chaud, X., Salama, K.: Physica C **181**, 81 (1991)
22. Petrisor, T., Giurgiu, A., Ciontea, L.: Appl. Supercond. **1**, 1219 (1993)
23. Abdelhadi, M.M., Ziq, Kh.A.: Supercond. Sci. Technol. **7**, 99 (1994)
24. Wu, N., Zern, H.H., Chen, C.: Physica C **241**, 198 (1995)
25. Joo, J., Kim, J.G., Nah, W.: Supercond. Sci. Technol. **11**, 645 (1998)
26. Altınkök, A., Yetiş, H., Kiliç, K., Kiliç, A., Olutaş, M.: Physica C **468**, 1419 (2008)
27. Foerstera, C.E., Lima, E., Rodrigues, P., Jr., Serbenaa, F.C., Lepienski, C.M., Cantao, M.P., Jurelo, A.R., Obradors, X.: Braz. J. Phys. **38**, 341 (2008)
28. Altinkok, A., Kiliç, K., Kiliç, A., Yetis, H., Olutas, M.: IEEE Trans. Appl. Supercond. **19**, 2978 (2009)
29. Azambuja, P., Rodrigues, P., Jr., Jurelo, A.R., Costa, R.M.: Braz. J. Phys. **40**, 195 (2010)
30. Day, M.J., Sutton, S.D., Wellhofer, F., Abell, J.S.: Supercond. Sci. Technol. **6**, 96 (1993)
31. dos Santos, C.A.M., da Luz, M.S., Ferreira, B., Machado, A.J.S.: Physica C **391**, 345 (2003)
32. Thinkam, M., Lobb, C.J.: Solid State Phys. **42**, 91 (1989)